Performance Analysis of a Dual input Non- isolated DC -DC Converter for Solar Powered Electric Vehicle

K. Arthi, S. Suja

*Department of Electrical & Electronics Engineering,
Coimbatore Institute of Technology, Coimbatore, Tamil Nadu,
INDIA-641014 (e-mail: arthi.k@cit.edu.in, suja@cit.edu.in).*

Abstract: The research work focuses on developing a Dual Input Non-Isolated Single Ended Primary Inductor converter (DINISC) sourced either from a Battery or Solar power or both to charge the EV (Electric Vehicle). The converter effectively uses solar power as one of its sources for charging the vehicle. To conquer challenges like fluctuating voltage range in solar panels, depleting battery charge and dynamic change in load requirements, the design and analysis of DINISC become essential in utilizing the available resources effectively. The DINISC is designed in such a way that it acts as a buffer taking in all the variations from the source side and our proposed DINISC is capable of delivering output power catering for the needs of the dynamic load. Since in an EV, the converter is the essential component, a complete analysis of the DINISC circuit becomes mandatory. Henceforth an in-depth small signal analysis under its various modes of operation along with stability concerns is addressed in our research work. A detailed software simulation is carried out in MATLAB –SIMULINK environment. The merits of the converter include high voltage gain, better efficiency, less ripples in the input side.

Keywords: Electric vehicle, DC-DC converter, solar PV, dual input, state space modelling.

1. INTRODUCTION

Globally EV Revolution has geared up to unleash the environment from pollution and save the ecosystem from carbon footprints that are being depleted by fossil fuel consumption. To avoid a rise in the utilization of fossil fuel based electricity generation, a Hybrid Energy System (HES) has been designed as an alternate method of energy production. HES can meet a variety of electricity needs in both urban and rural areas. Hybridization is a combination of Photo Voltaic (PV)/wind, fuel cell/solar PV, ultra capacitor/battery, and other technologies. An appropriate Power Electronic Interface (PEI) must be adopted for optimum use of HES to balance the production from intermittent sources such as PV and Wind with user requirements (Luis et al., 2011).

As a result, power converters are designed in such a way to combine different renewable energy sources due to their compact structure, affordable price and low complexity. The integration of Solar Photo Voltaic (SPV) technology into Electric Vehicles (EVs) is a significant challenge for experts, mostly due to the stochastic nature of sun irradiance (Paul Arevalo et al., 2021).

In contrast to single-input converters, multiple input converters with supplemental sources are taken into consideration to incorporate hybrid energy sources. Historically, numerous studies addressing independent single input single output DC-DC converters have been presented. This strategy leads to a rise in both the cost and quantity of semiconductor components, thus resulting in an escalation of component loss (Ankit et al., 2020). As reported (Moumita et al., 2023, Michelangelo et al., 2016, Muhammad et al., 2020), a vehicle solely operating on solar power for charging the vehicle battery is been developed. Solar energy, as widely acknowledged, is abundantly available in nature. However, due to its intermittent characteristics, it becomes necessary to depend on supplementary sources.

The integration of dual sources like onboard solar PV with the grid, will lead to significant problems in the power grid. Dual-input DC-DC converters can solve the difficulty of combining energy sources for EV charging (Gangavarapu et al., 2019). A variety of DC- DC Converters are found in the literature with various combinations of buck converter, boost converter and buck-boost converter.

The Dual Input Single Output converter architecture is developed to integrate two input sources. This converter utilizes both solar PV and battery power in six modes of operation (Gangavarapu et al., 2022).

Work in (Kuditi et al., 2021) discusses on Dual input converters for the buck, boost, & buck-boost are modeled and analyzed by demonstrating their ability to maintain a constant output voltage under varying source conditions for sustainable EV charging. To optimize their potential as future modes of transportation, an in depth analysis of Electric vehicle source combinations, models, Energy Management Systems (EMS) and control algorithms are addressed. However, there are notable areas in terms of both dependability and intelligent systems, indicating that additional enhancements are indispensable (Hannan et al., 2021).

In (Alexis, 2009), suggests four guidelines for determining single input, that can be adapted to Multiple Input Converter (MIC) topologies. The rules are guidelines for designing a MIC in such a way that it meets certain assumptions, restrictions and conditions, independent control of input sources, control of each input separately, proper isolation, common stage input capacitor has to distributed among input cells and thus minimizing the total number of components. They provide a framework for designing efficient multiple input converters while avoiding common pitfalls and ensuring proper functionality. Research work (Sanjida et al., 2021) describes about multiport fly back converter with a SPV Battery capable of MPP tracking for each module where the bidirectional capability of the converter is not appreciated.

A multi input multi output DC-DC Single Ended Primary Inductor converter (SEPIC) based three port converter (Arun et al., 2023) with four switches and four diodes is proposed for EV charging, with solar PV as the primary source to charge the battery and a novel power flow control based on time sharing in conjunction with mode specific voltage regulation. A four port (Aravind et al., 2023) converter with improved efficiency and high voltage gain with single output topology is discussed with more active components compared to the proposed converter.

Fuel cells and solar photovoltaic (SPV) panels are actively supported by (Saikumar et al., 2023; Pawan et al., 2022) the converter, which makes use of the concept of multiple switching frequencies to achieve extensive control over output voltage and power flow. An innovative architecture for EV traction systems that leverages 48V battery packs and multi input high conversion ratio converters. It achieves high gain, supports variable DC link applications and simplifies battery management while maintaining safety and enabling DC fast charging (Ankul et al., 2021).

A Zero Voltage Transition (ZVT) non-isolated high-voltage gain dual-input DC/DC converter with improved conversion efficiency with more components (Binxin et al., 2019). A non isolated converter with two stage boost converter at the input stage which can be used as single input or in interleaved manner. The converter improves the voltage gain through Diode capacitor clamped voltage multiplier circuit (Venkata et al., 2016).

Grid connected converter for hybrid system which is been supplied through PV, wind and Battery energy storage system (Ridha, 2019) are various converter topologies surveyed in the literature. In the work (Yan et al., 2010), the author explores the synthesis on multi input DC converter, by providing insights into their design by allowing the dual input to operate individually to obtain simultaneous power and sequential flow of power which permits only one source to power the load.

Thus literature shows that EVs will make a paradigm shift towards Zero Consumption of fossil fuel which leads to a reduction of Greenhouse Gas (GHG) emissions by enhancing a pollution-free environment. Practically EV's depend on a Grid to charge them but it faces several issues a) the conventional power grid is powered by Conventional Energy sources like thermal power plants, diesel plants, and nuclear plants where the adoption towards EVs has no significance b) Charging an electric vehicle during peak hours, whether before departing home or upon returning from work, poses a significant risk of adversely affecting the grid. Countries like India has substantial solar irradiation, with several locations receiving more than 80% of days in a year of sunlight which makes solar energy as reliable source for Electric Vehicle charging thereby reducing dependence on the conventional grid.

The organization of the paper is as follows, section 2 discusses on architecture of the converter and section 3 discusses on modes of operation for the SEPIC converter under different operating conditions, and section 4 explains small signal modelling of converters in charging and discharging states under conditions like as explained in section 3,section 5 explain about the control mechanism of the proposed converter, section 6 explains about results & discussion and finally research work is concluded in section 7.

2. ARCHITECTURE OF THE CONVERTER

From various literature, single or multi input converter topologies that are proposed, emerge from the basic inspiration towards charging the inductor, hence these inductors can be charged from source to load through multiple or single sources.

The Challenge of the Proposed Converter is that irrespective of the Input Parameters the Converter is supposed to deliver a Ripple Free Constant DC Voltage to the EV motor through suitable motor driver to operate the vehicle. The SEPIC converter can be able to operate in both boost as well as buck converter modes. The operation of it depends on the duty ratio whether it's greater than 50% or lesser. In conventional configuration as in Fig.1a the converter requires more than one converter which increases the complexity to operate in the describe four different modes, rather in proposed configuration Fig.1b shows of a single converter which will perform all the four different modes of operation.

Designing a converter to deliver a ripple-free constant DC voltage is necessary since the converter must deliver a stable output regardless of input voltage and load variations, catering for the requirement, Fig. 1c shows the architecture of the dual input converter for EV application. The proposed circuit incorporates only three IGBT switches, two without anti-parallel diode (S_b, S_{PV}), a switch with anti-parallel diode (S_{sep}), diode D_1, D_2, a freewheeling diode D_{Sep}, Inductors L_1, L_2, coupling capacitor (C_1) and output capacitor (C_2). The switch without anti parallel diode is to ensure unidirectional current flow. The work mainly aims at integrating two energy sources supplying energy to the load. The converter operates in the following modes

i. Battery powering the vehicle
ii. Solar PV and Battery powering the Vehicle
iii. Solar PV powered Vehicle

3. MODES OF OPERATION OF THE CONVERTER

The topology employs a SEPIC-based converter rather than a generic buck-boost converter due to its additional benefits of non-inverted output and reduced input ripple current as a result which leads to reduced EMI. The dual input SEPIC converter has been designed specifically to effectively manage two input sources, enabling the switching between the sources or the ability to combine power from two distinct sources providing a good degree of fault tolerance.

The input side Inductor voltage and current variations are shown in Fig 2. For analysis of DINISC the two input sources, a battery and Solar PV are considered with a condition that $V_b > V_{PV}$.

Power flow is considered in this converter where either V_b or V_{PV} will be charging or both the sources will be charging the vehicle for complete propulsion. The power flow towards the load is controlled by switches S_b, S_{PV}, S_{sep}.

The inductor L_1 charges when the switch S_{sep} is ON and the coupling capacitor C_1 discharges its stored energy to inductor L_2. The effectiveness of the converter is that it can energize the input inductor L_1 either individually or simultaneously through the switches S_b and S_{PV}. On completion of the charging cycle, the output capacitor C_2 delivers its stored energy to the load by turning ON D_{sep} and S_{sep} OFF.

The analytical equations of the converter working under charging & discharging modes are explained in the following section. Based on the switching pattern the DINISC has the following modes of operation

MODE I -Battery Powered Vehicle mode (BPV): The EV battery alone is used for propulsion of the vehicle. During non sunny days or in winter the vehicle is made to operate in this mode.

MODE II-Hybrid Mode: The combined power of solar and battery propels the EV forward. This mode enables the EV to utilize the solar energy and battery power so that maximum energy can be harnessed in the vehicle and further excess energy utilized for auxiliary needs.

MODE III-Solar PV Powered mode (SPV): During sunny days the converter operates in Single input mode where the PV generated locally is utilized to continue the propelling of the vehicle.

Mode III operation will be carried out when solar power irradiation is sufficient to supply the vehicle for acceleration. Switching loss and resistive drop of passive components are considered to be insignificant in DINISC analysis.

The dual input converter improves vehicle propelling efficiency by supplying power to the load continuously regardless of whether a power source fails. Analysis of the SEPIC converter has been carried out in dynamic and steady state conditions. Table 1 shows different operating states of the proposed converter.

Interval 1(0≤Ts≤T1): During this period**,** switches S_b, S_{sep}, D_2 are ON and S_{PV}, D_1 are in OFF conditions, equivalent circuit of the converter is shown in Fig.3a.

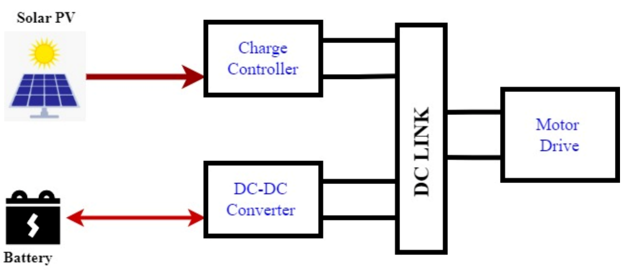

(a)

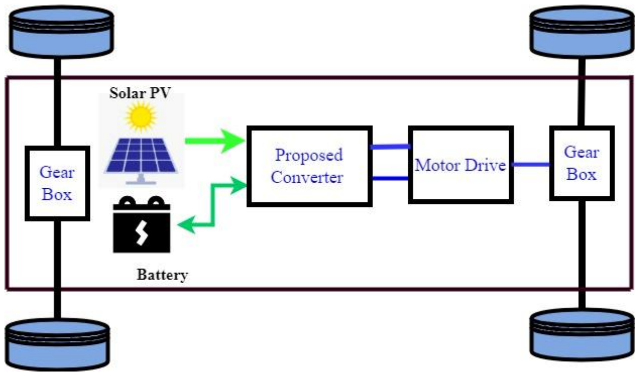

(b)

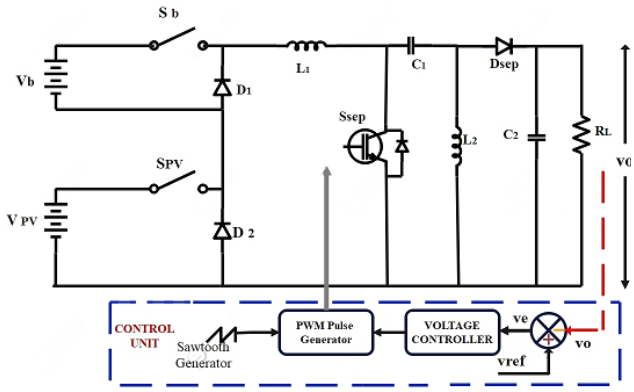

(c)

Fig. 1. (a) Conventional Configuration of Dual input EV
(b) Proposed Configuration of Dual input EV
(c) Architecture of DINISC.

Such that the first source V_b delivers energy to charge the inductor L_1, current through inductor increases linearly from its initial value i_{L0}. In this period current through the inductor L_1 is indicated in (1) which is given as

$$i_{L1}=i_{L0}+\frac{1}{L_1}\int_0^{d_1T_s} V_{L1}\,dt$$

$$i_{L1}=i_{L0}+\frac{1}{L_1}V_{L1}d_1Ts=i_{L0}+\frac{1}{L_1}V_b\,d_1Ts \quad (1)$$

Interval 2(T1≤Ts≤T2): In this period, switches S_b, S_{sep} are ON and D_1, D_2 is OFF, equivalent circuit of the converter is shown in Fig.3c. The voltage across the inductor is $V_b + V_{PV}$ and current through inductor L_1 is $i_{(b+PV)}$. By applying dual sources current through inductor increase, slope increases when compared to previous period. Current flowing through inductor in this mode is given in (2)

$$i_{L1}=i_{L(1)}+\frac{1}{L_1}\int_{d_1T_s}^{d_2T_s} V_{L1}\,dt$$

$$i_{L1}=i_{L(1)}+\frac{1}{L_1}(V_b+V_{PV})*(d_2-d_1)Ts \quad (2)$$

Here $V_{L1}=(V_b+V_{PV})$

*Interval 3(T2≤Ts≤T3)***:** In this period, switches S_{PV}, S_{sep}, D_1 are ON and S_b, D_2 is OFF, equivalent circuit of the converter is shown in Fig.3b. The voltage across the inductor is V_{PV} and current through inductor L_1 is $i_{(PV)}$. Current flowing through inductor in this mode is given in (3)

$$i_{L1}=i_{L0}+\frac{1}{L_1}\int_{d_2T_s}^{d_3T_s} V_{L1}\,dt$$

$$i_{L1}= i_{L(2)}+\frac{1}{L_1}(V_{PV}) *(d_3-d_2)T_s \tag{3}$$

Here $V_{L1} = V_{PV}$

During charging of L_1 from the dual sources, capacitor C_1 discharges its stored energy to inductor L_2 and where C_2 energies its electrostatic stored energy to the load.

Interval 4(T3≤Ts≤T4): In this period energy stored in inductor L_1 is transferred to load through C_2. Switches S_{PV}, S_b, D_{sep} are in ON state and D_1, D_2, S_{sep} are in OFF state, and equivalent circuit of this state is shown in Fig.3d. During this state, current through capacitor C_1 is equal to the inductor current i_{L1}

$$i_{L1}=i_{L0}+\frac{1}{L1}\int_{d_3T_s}^{d_4T_s} V_{L1}\, dt$$

$$i_{L1}= i_{L(3)}-\frac{1}{L_1}(V_b+V_{PV}) *(d_4-d_3)T_s \tag{4}$$

Table 1. Different Operating States of the Converter.

Operating modes	Operating switch	Voltage across Inductor L1	Status
Period 1	S_b,S_{sep},D_2	V_b	Charging
Period 2	S_{PV}, S_b, S_{sep}	V_b+V_{PV}	Charging
Period 3	S_b, S_{sep},D_1	V_{PV}	Charging
Period 4	S_{PV}, S_b, D_{sep}	V_b+V_{PV}	Discharging

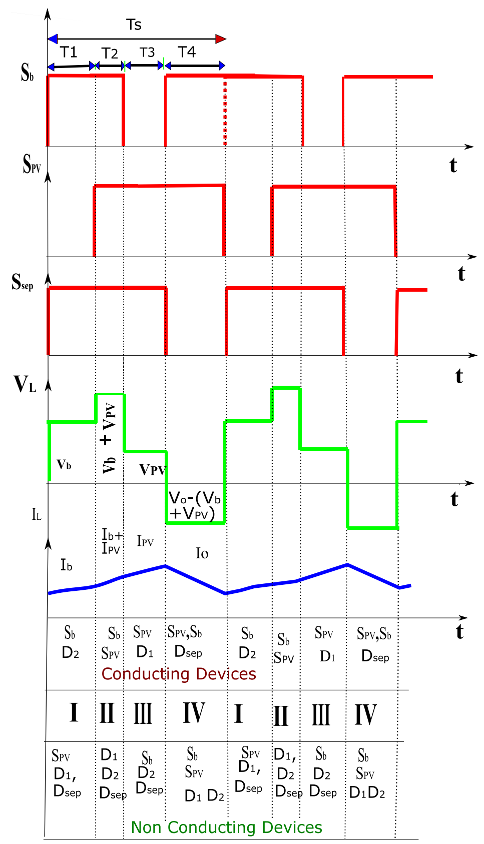

Fig. 2. Switching Waveforms of Dual Input Non Isolated SEPIC.

The inductor current decreases from previously stored energy. The average voltage across the inductor for a cycle is zero as volt-second balance equation, which is written as follows

$$V_b*d_1+ (V_{PV}+ V_b)*(d_2-d_1) + V_{PV}*(d_3-d_2) + (V_{PV}+V_b-V_0)*(1-d_3-d_2-d_1) =0; \tag{5}$$

$$\text{Where } d_1=\frac{T1}{Ts};\ d_2=\frac{T2}{Ts};\ d_3=\frac{T3}{Ts};\ d_4=\frac{T4}{Ts}=\frac{Ts}{Ts}=1;$$

where $1-d_3$ is the duty cycle of switch S_b, $1-d_1$ is the duty cycle of switch S_{PV}, $d_1+d_2+d_3$ is the duty cycle of switch S_{sep}.

Switch S_b will conduct from t=0 to T2, switch S_{PV} will conduct from the period t=T1 to T3, switch S_{sep} will conduct from the period t=0 to T3.

From (1)-(5), output voltage V_o of DINISC can be written as

$$V_o=\frac{V_b(1-d_1-d_3)+V_{PV}(1-2d_1-d_2)}{(1-d_1-d_2-d_3)} \tag{6}$$

4. SMALL SIGNAL MODELLING OF DUAL INPUT NON ISOLATED SEPIC CONVERTER

The DC-DC converters often exhibit intricate and non-linear characteristics as a result of its switching operation and energy storage components (L/C). The state space averaging technique is utilized as a foundation for deriving the linear model of DC-DC converters, which establishes the relationship between input-output characteristics and control qualities. The insights that emerge from state space modelling approach results in developing the dynamic equation of the converter (Erickson, 2001).

The DINISC operation is categorized in four different states based on which source is energizing the inductor as whether S_b or S_{PV} or both will be ON for part of the time period which are shown in Fig.3.

The generalized state space representation is given as

$$\dot{x}(t)=A\, x(t) +B\, u(t)$$

$$y=C\, x(t) +D\, u(t) \tag{7}$$

where x (t) is state variable matrix , u(t) is input variable and y is output equation.

$$x(t)=\begin{bmatrix} i_{L1} \\ i_{L2} \\ V_{C1} \\ V_{C2} \end{bmatrix},\ \dot{x}(t)=\begin{bmatrix} \dot{i}_{L1} \\ \dot{i}_{L2} \\ \dot{V}_{C1} \\ \dot{V}_{C2} \end{bmatrix},\ u(t)=\begin{bmatrix} V_{PV} \\ V_b \end{bmatrix}\ y=\begin{bmatrix} i_{PV} \\ i_b \\ i_{(PV+b)} \\ V_0 \end{bmatrix}$$

During mode I, as shown in Fig.3a, S_{sep} switch ON by allowing battery to charge the inductor from the time t=0 to T1. The state space and output equation of converter for this mode I is

$$\begin{bmatrix} \dot{i}_{L1} \\ \dot{i}_{L2} \\ \dot{V}_{C1} \\ \dot{V}_{C2} \end{bmatrix}=\begin{bmatrix} 0 & 0 & 0 & 0 \\ 0 & 0 & 0 & 0 \\ 0 & 0 & 0 & 0 \\ 0 & 0 & 0 & \frac{-1}{C_2R_L} \end{bmatrix}\begin{bmatrix} i_{L1} \\ i_{L2} \\ V_{C1} \\ V_{C2} \end{bmatrix}+\begin{bmatrix} 0 & \frac{1}{L1} \\ 0 & 0 \\ 0 & 0 \\ 0 & 0 \end{bmatrix}\begin{bmatrix} V_{PV} \\ V_b \end{bmatrix} \tag{8}$$

Output equation

$$\begin{bmatrix} i_{PV} \\ i_b \\ i_{PV+b} \\ V_0 \end{bmatrix} = \begin{bmatrix} 0 & 0 & 0 & 1 \\ 0 & 0 & 0 & 0 \\ 1 & 0 & 0 & 0 \\ 0 & 0 & 0 & 0 \end{bmatrix} \begin{bmatrix} i_{L1} \\ i_{L2} \\ V_{C1} \\ V_{C2} \end{bmatrix} + \begin{bmatrix} 0 & 0 \\ 0 & 0 \\ 0 & 0 \\ 0 & 0 \end{bmatrix} \begin{bmatrix} V_{PV} \\ V_b \end{bmatrix} \qquad (9)$$

In mode II as shown in Fig.3c, S_{sep} is ON and Solar PV is made to supply the load along with the battery from time t=T1 to T2, current through the inductor L_1 is $i_{(PV+b)}$ and voltage across inductor is $V_b + V_{PV}$. Due to addition of dual sources, the inductor current slope is larger compared to previous interval.

The state space and output equation of converter for this mode II is given below

$$\begin{bmatrix} \dot{i}_{L1} \\ \dot{i}_{L2} \\ \dot{V}_{C1} \\ \dot{V}_{C2} \end{bmatrix} = \begin{bmatrix} 0 & 0 & 0 & 0 \\ 0 & 0 & \frac{1}{L_2} & 0 \\ 0 & \frac{-1}{C_1} & 0 & 0 \\ 0 & 0 & 0 & \frac{-1}{C_2 R_L} \end{bmatrix} \begin{bmatrix} i_{L1} \\ i_{L2} \\ V_{C1} \\ V_{C2} \end{bmatrix} + \begin{bmatrix} \frac{1}{L_1} & \frac{1}{L_1} \\ 0 & 0 \\ 0 & 0 \\ 0 & 0 \end{bmatrix} \begin{bmatrix} V_{PV} \\ V_b \end{bmatrix} \qquad (10)$$

Output equation

$$\begin{bmatrix} i_{PV} \\ i_b \\ i_{PV+b} \\ V_0 \end{bmatrix} = \begin{bmatrix} 0 & 0 & 0 & 1 \\ 0 & 0 & 0 & 0 \\ 0 & 0 & 0 & 0 \\ 1 & 0 & 0 & 0 \end{bmatrix} \begin{bmatrix} i_{L1} \\ i_{L2} \\ V_{C1} \\ V_{C2} \end{bmatrix} + \begin{bmatrix} 0 & 0 \\ 0 & 0 \\ 0 & 0 \\ 0 & 0 \end{bmatrix} \begin{bmatrix} V_{PV} \\ V_b \end{bmatrix} \qquad (11)$$

In mode III, as shown in Fig.3b , S_{sep} is ON, the system is powered entirely through solar PV and the Battery is kept in OFF state throughout this mode of operation with its time period from t=T2 to T3.

The state space and output equation of converter for mode III operation is given as

$$\begin{bmatrix} \dot{i}_{L1} \\ \dot{i}_{L2} \\ \dot{V}_{C1} \\ \dot{V}_{C2} \end{bmatrix} = \begin{bmatrix} 0 & 0 & 0 & 0 \\ 0 & 0 & \frac{1}{L_2} & 0 \\ 0 & \frac{-1}{C_1} & 0 & 0 \\ 0 & 0 & 0 & \frac{-1}{C_2 R_L} \end{bmatrix} \begin{bmatrix} i_{L1} \\ i_{L2} \\ V_{C1} \\ V_{C2} \end{bmatrix} + \begin{bmatrix} \frac{1}{L_1} & 0 \\ 0 & 0 \\ 0 & 0 \\ 0 & 0 \end{bmatrix} \begin{bmatrix} V_{PV} \\ V_b \end{bmatrix} \qquad (12)$$

Output equation

$$\begin{bmatrix} i_{PV} \\ i_b \\ i_{PV+b} \\ V_0 \end{bmatrix} = \begin{bmatrix} 0 & 0 & 0 & 1 \\ 1 & 0 & 0 & 0 \\ 0 & 0 & 0 & 0 \\ 0 & 0 & 0 & 0 \end{bmatrix} \begin{bmatrix} i_{L1} \\ i_{L2} \\ V_{C1} \\ V_{C2} \end{bmatrix} + \begin{bmatrix} 0 & 0 \\ 0 & 0 \\ 0 & 0 \\ 0 & 0 \end{bmatrix} \begin{bmatrix} V_{PV} \\ V_b \end{bmatrix} \qquad (13)$$

During the period from T3 to T4 (T_s), the solar PV and battery freewheels the supply towards the load by turning OFF S_{sep} which is depicted in Fig.3d. The corresponding state equation and output equation are

$$\begin{bmatrix} \dot{i}_{L1} \\ \dot{i}_{L2} \\ \dot{V}_{C1} \\ \dot{V}_{C2} \end{bmatrix} = \begin{bmatrix} 0 & 0 & \frac{-1}{L_1} & \frac{-1}{L_1} \\ 0 & 0 & 0 & \frac{-1}{L_2} \\ \frac{1}{C_1} & 0 & 0 & 0 \\ \frac{1}{C_2} & \frac{1}{C_2} & 0 & \frac{-1}{C_2 R_L} \end{bmatrix} \begin{bmatrix} i_{L1} \\ i_{L2} \\ V_{C1} \\ V_{C2} \end{bmatrix} + \begin{bmatrix} \frac{1}{L_1} & \frac{1}{L_1} \\ 0 & 0 \\ 0 & 0 \\ 0 & 0 \end{bmatrix} \begin{bmatrix} V_{PV} \\ V_b \end{bmatrix} \qquad (14)$$

Output equation is

$$\begin{bmatrix} i_{PV} \\ i_b \\ i_{PV+b} \\ V_0 \end{bmatrix} = \begin{bmatrix} 0 & 0 & 0 & 1 \\ 0 & 0 & 0 & 0 \\ 0 & 0 & 0 & 0 \\ 1 & 0 & 0 & 0 \end{bmatrix} \begin{bmatrix} i_{L1} \\ i_{L2} \\ V_{C1} \\ V_{C2} \end{bmatrix} + \begin{bmatrix} 0 & 0 \\ 0 & 0 \\ 0 & 0 \\ 0 & 0 \end{bmatrix} \begin{bmatrix} V_{PV} \\ V_b \end{bmatrix} \qquad (15)$$

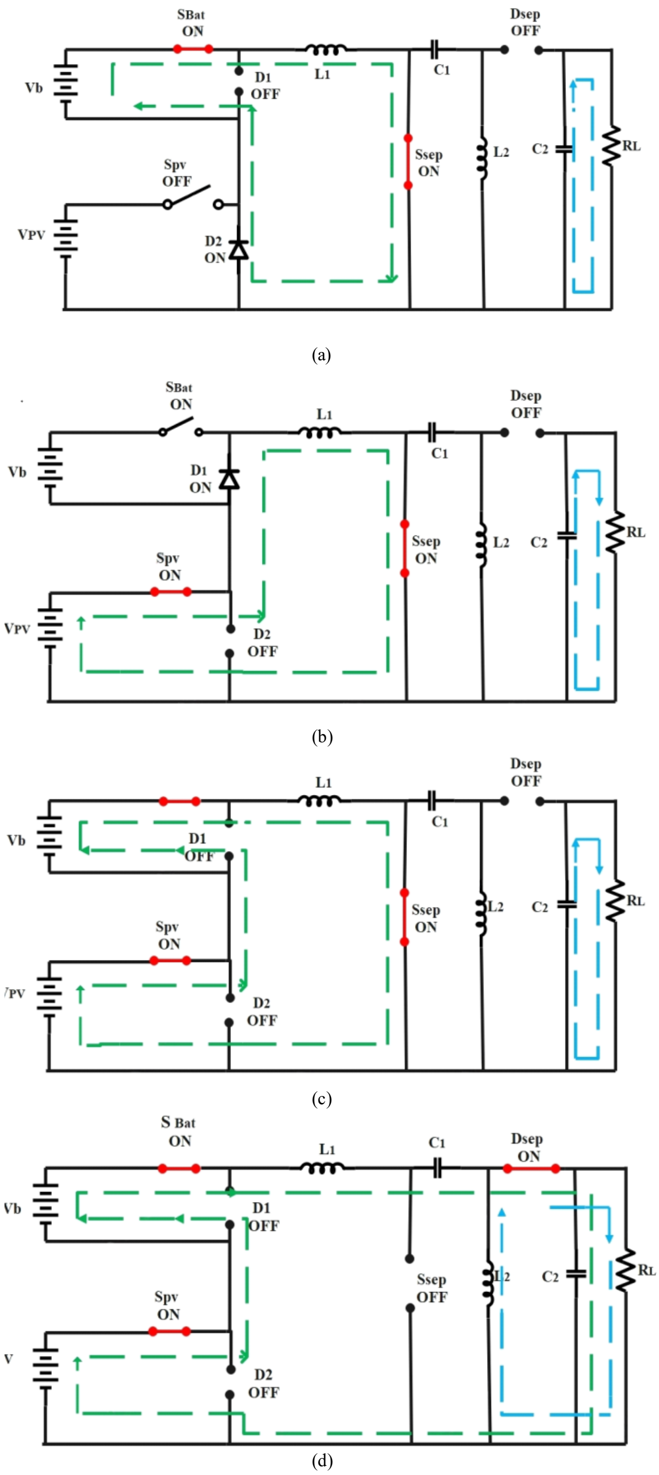

Fig. 3. Charging of Inductor L_1 in (a) Battery powered mode, (b) Solar powered Mode, (c) Hybrid mode, (d) Discharging of Inductor to load R_L.

With these expressions (8) – (15) average large signal state equations are derived and the final values A, B, C, and D are as follows

$$A=\begin{bmatrix} 0 & 0 & \frac{-(1-d_3)}{L_1} & \frac{-(1-d_3)}{L_1} \\ 0 & 0 & \frac{d_3}{L_2} & \frac{-(1-d_3)}{L_2} \\ \frac{(1-d_3)}{C_1} & \frac{-d_3}{C_1} & 0 & 0 \\ \frac{(1-d_3)}{C_2} & \frac{(1-d_3)}{C_2} & 0 & \frac{-1}{C_2R_L} \end{bmatrix};\ B=\begin{bmatrix} \frac{(1-d_1)}{L_1} & \frac{1+d_2+d_3}{L_1} \\ 0 & 0 \\ 0 & 0 \\ 0 & 0 \end{bmatrix};$$

$$C=\begin{bmatrix} 0 & 0 & 0 & 1 \\ d_3-d_2 & 0 & 0 & 0 \\ d_1 & 0 & 0 & 0 \\ 1+d_2-d_1-d_3 & 0 & 0 & 0 \end{bmatrix}$$

The state variables have time-varying quantities, which causes non-linearity. In order to obtain the system's linear, an AC perturbation of a small signal is superimposed in current, voltage, and duty cycles ie) $V+\hat{v}$, $I+\hat{i}$ & $d+\hat{d}$.

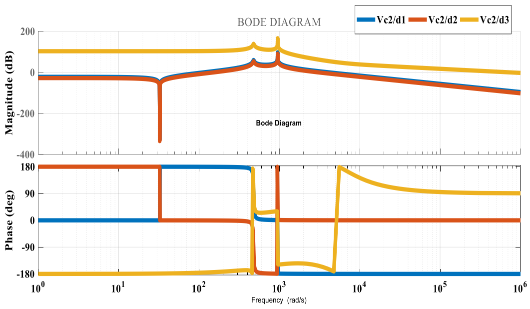

Fig. 4. Bode plot for the transfer functions $\frac{v_{c2}(s)}{\hat{d}_1(s)}, \frac{v_{c2}(s)}{\hat{d}_2(s)}, \frac{v_{c2}(s)}{\hat{d}_3(s)}$.

Small signal analysis is a technique for understanding and designing a system, by linearizing a system's behaviour around an operating point and analyzing its response to small perturbations. Therefore the state space model for the linearised DINISC is given by

$$\dot{x}(t)=A\,x(t)+Bu(t)+Ed_1+Fd_2+Gd_3$$

$$Y = C\,x(t)+Du(t)+Hd_1+Id_2+Jd_3 \tag{16}$$

The coefficients E, F, G, H, I, J of the state equations are as follows

$$\left.\begin{aligned} E&=(A_1-A_2)X+(B_1-B_2)U \\ F&=(A_2-A_3)X+(B_2-B_3)U \\ G&=(A_3-A_4)X+(B_3-B_4)U \\ H&=(C_1-C_2)X+(D_1-D_2)U \\ I&=(C_2-C_3)X+(D_2-D_3)U \\ J&=(C_3-C_4)X+(D_3-D_4)U \end{aligned}\right\} \tag{17}$$

The small signal state space model for DINISC can be obtained by substituting the values of E, F, G, H, I, J using (16) and (17) which is expressed as follows.

The transfer function of the dual input converter can be extracted by perturbing the voltage sources and duty ratios. The design parameters are listed in Table 2 by considering change in supply voltage due to intermittent solar power, varying battery voltage and dynamic load. The transfer function $\frac{v_{c2}(s)}{\hat{d}_1(s)}$ is obtained in s domain by making v_{PV}, v_b, d_2, d_3 quantities as zero.

$$\begin{bmatrix} \dot{\hat{i}}_{L1} \\ \dot{\hat{i}}_{L2} \\ \dot{\hat{V}}_{C1} \\ \dot{\hat{V}}_{C2} \end{bmatrix} = \begin{bmatrix} 0 & 0 & \frac{-(1-d_3)}{L_1} & \frac{-(1-d_3)}{L_1} \\ 0 & 0 & \frac{d_3}{L_2} & \frac{-(1-d_3)}{L_2} \\ \frac{(1-d_3)}{C_1} & \frac{d_3}{C_1} & 0 & 0 \\ \frac{(1-d_3)}{C_2} & \frac{(1-d_3)}{C_2} & 0 & 0 \end{bmatrix} \begin{bmatrix} \hat{i}_{L1} \\ \hat{i}_{L2} \\ \hat{V}_{C1} \\ \hat{V}_{C2} \end{bmatrix} + \begin{bmatrix} \frac{1-d_1}{L_1} & \frac{1+d_2-d_3}{L_1} \\ 0 & 0 \\ 0 & 0 \\ 0 & 0 \end{bmatrix} \begin{bmatrix} \hat{V}_{PV} \\ \hat{V}_b \end{bmatrix} + \begin{bmatrix} \frac{V_{PV}}{L_1} \\ 0 \\ 0 \\ 0 \end{bmatrix} \hat{d}_1 + \begin{bmatrix} \frac{V_b}{L_1} \\ 0 \\ 0 \\ 0 \end{bmatrix} \hat{d}_2 + \begin{bmatrix} \frac{(V_{C1}+V_{C2}-V_b)}{L_1} \\ \frac{(V_{C1}+V_{C2})}{L_2} \\ \frac{-(i_{L1}+i_{L2})}{C_1} \\ \frac{-(i_{L1}+i_{L2})}{C_2} \end{bmatrix} \hat{d}_3 \tag{18}$$

Table 2. Simulation Parameters.

Parameters	Specifications
Source V_b(Battery)	48V
Source V_{PV}(Solar PV)	24V
Maximum voltage V_{max} of PV	40.9V
Open circuit voltage V_{oc} of PV	48.9V
Short Circuit Current I_{sc} of PV	11.32
Power P_{max} of PV	445W
Inductor L_1,L_2	0.417mH
Capacitor C_1,C_2	20µF,41.6µF
Switching frequency	20kHz
Load Resistance	38Ω
Output Voltage	120V

Similarly other transfer functions are obtained $\frac{v_{c2}(s)}{\hat{d}_2(s)}, \frac{v_{c2}(s)}{\hat{d}_3(s)}$

$$\frac{v_{c2}(s)}{\hat{d}_1(s)} = \frac{-V_{PV}(1-D_3)(s^2C_1+K+J)}{s^4L_1C_1C_2+\frac{s^3L_1C_1}{R_L}+s^2L_1(C_2K+C_1M)+\frac{sL_1K}{R_L}+L_1(MK-J^2)} \tag{19}$$

$$\frac{v_{c2}(s)}{\hat{d}_2(s)} = \frac{V_b(1-D_3)(s^2C_1+K+J)}{s^4L_1C_1C_2+\frac{s^3L_1C_1}{R_L}+s^2L_1(C_2K+C_1M)+\frac{sL_1K}{R_L}+L_1(MK-J^2)} \tag{20}$$

$$\frac{v_{c2}(s)}{\hat{d}_3(s)} = \frac{(X-s(i_{L1}+i_{L2}))(s^2C_1+K+J)+Z(s^2C_1+K)-JY}{s^4C_1C_2+\frac{s^3C_1}{R_L}+s^2(C_2K+C_1M)+\frac{s^*K}{R_L}+(MK-J^2)} \tag{21}$$

Where $K=\frac{D_3^2}{L_1}+\frac{D_3^2}{L_2}$, $M=\frac{D_3^2}{L_1}+\frac{(1-D_3)^2}{L_2}$,

$J=\frac{-(1-D_3)^2}{L_1}+\frac{D_3(1-D_3)}{L_2}$, $X=\frac{(1-D_3)(V_{c1}+V_{C2}-V_B)}{L_2}$,

$Y=\frac{D_3(V_{C1}+V_{C2})}{L2}$, $Z=\frac{(1-D_3)}{L_2}$

From the bode plot as shown in Fig.4 it is observed that system gain margin and phase margin of the DINIS Converter are 192 db and -90.2° respectively. To analyze the stability of the proposed converter by relative stability the poles of the transfer function is to be in left half of S plane. Eigen values of the converter are calculated using matrix A, and whose Eigen values are -1.5±j 952.8 and - 5.53±j477.95, which shows the converter stays in stable region.

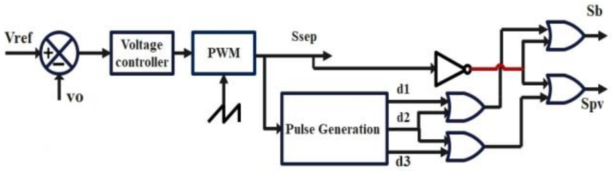

Fig. 5. Control strategy for pulse production to Switches for DINISC in hybrid mode.

5. CONVERTER CONTROL

Based on Average Current mode control (ACM) (Maheswari Ellappan et al., 2020& R.Munuswamy et al., 2020) which is used to design control strategy for a typical power electronic converter. This control includes control on load side or source side. The proposed strategy uses load side control, where the outer voltage loop is taken into account to regulate load voltage.

As the main aim of the work is to obtain a constant output voltage for vehicular application, this paper utilizes voltage loop control. The output v_o is measured and compared with v_{ref}, a voltage error of v_e is estimated

$$v_e(k)=v_{ref}(k)-v_o(k) \tag{22}$$

where (k) indicates the sampling instant.

From the error voltage, control signal v_{ct} is estimated at the output through PI controller.

$$v_{ct}(k)= v_{ct}(k-1)+k_p\{v_e(k)-v_e(k-1)\}+k_i * v_e(k) \tag{23}$$

Here k_p and k_i are tuned proportional (P) and integral (I) gain constants. PI controller is used to maintain constant output voltage by minimizing the error.

The PI controller values are found using Ziegler-Nicholas method to achieve the charging voltage of 120volts. Further any advanced soft-computing-based tuning strategies can enhance PI controller effectiveness.

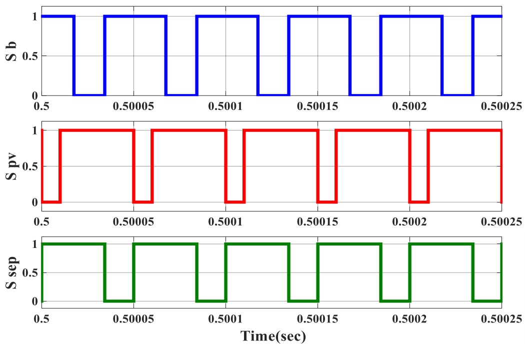

Fig. 6. Switching signal for DINIS converter in Hybrid Mode.

Pulse Width Modulation (PWM) pulses for the DINISC converter is generated by the controllers based on the error from comparison between the actual output and reference. The switching technique is chosen based on the power consumption of the energy sources, whether they are distributed separately or concurrently. Intermediate pulse generation for dual input converter (Yan Li et al., 2010) is been considered.

Fig. 5 shows the control strategy for pulse production to DINISC during hybrid mode of operation. The pulse generation for switches S_b and S_{PV} is obtained by identifying the duty cycle of S_{sep}.

By considering the S_{sep} pulse as base, delays for other modes are obtained. The total time period of the SEPIC switch is equal to the time period of all the switches but the ON period of SEPIC will not be greater the ON period of S_b and S_{PV}. During mode IV, the energy from inductor, battery and solar are made to flow towards the load and also it charges the inductor L_2 & C_2 . The stored energy in these two passive components can be utilized when inductor L_1 is at charging mode.

6. RESULTS & DISCUSSIONS

The performance of the dual input converter has been validated using MATLAB/SIMULINK environment and the parameters considered for simulation are listed in Table 2. A battery of 48V DC and solar PV of 24volts are the Dual input of the converter with load resistor of 38 ohms is taken into consideration for the simulation study.

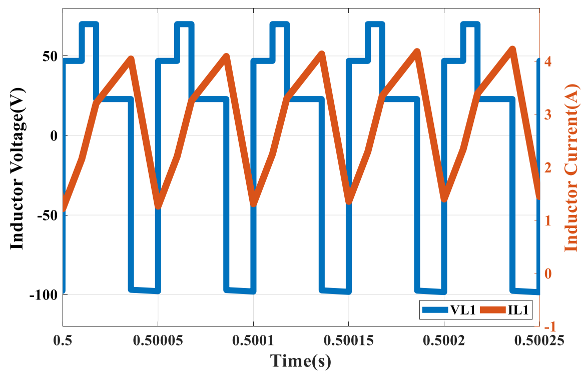

(a)

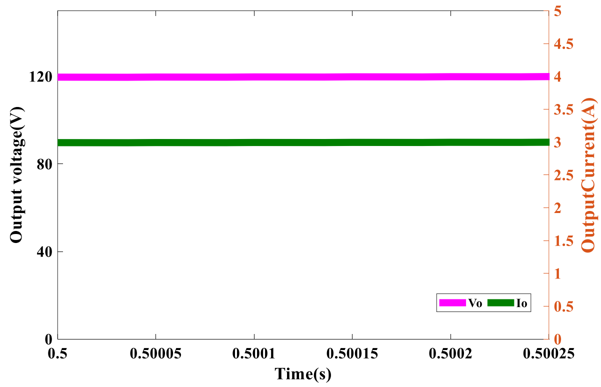

(b)

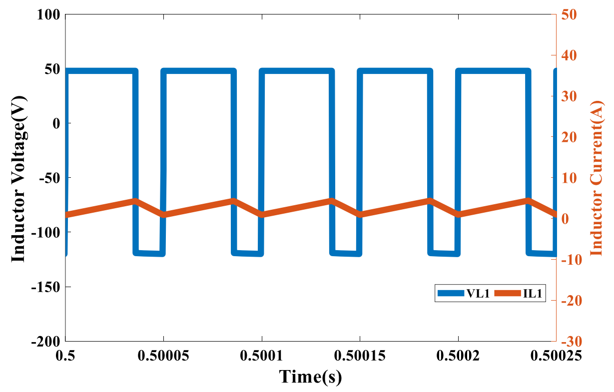

(c)

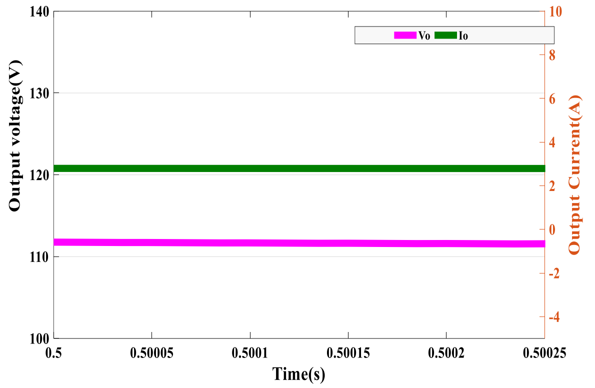

(d)

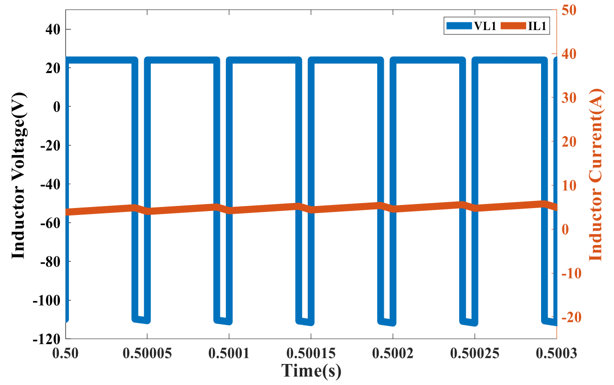

(e)

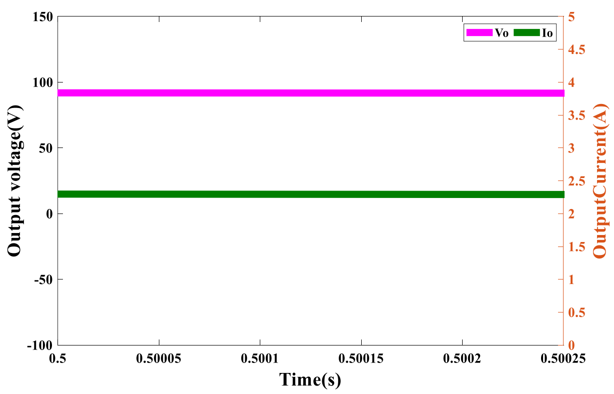

(f)

Fig.7. Simulation results of DINISC when power flow is from source to load. a) Inductor voltage and current during hybrid mode ,b) Output voltage and current during hybrid mode , c) Inductor voltage and current during BPV, d) Output voltage and current during BPV, e) Inductor voltage and current during SPV, f) Output voltage and current during SPV.

A filter capacitor of 41.6μF is designed such that the ripple in the output voltage is less than 3% which is desired and expected value. In Fig.6 shows the switching pulses for the dual input converter for the switches S_b, S_{PV}, S_{sep}. The simulation results of the inductor L_1 charging are clearly depicted in the output waveforms of Fig.7. During battery powered vehicle mode the charging of inductor L_1, output voltage and output current are shown in Fig. 7c&7d.

During mode 2 the charge in L_1 gets with the added power from solar PV, the cumulative power of both sources makes the independently on Solar PV alone for duration of d_3%. The inductor current and output voltage waveforms are shown in Fig. 7a&7b.

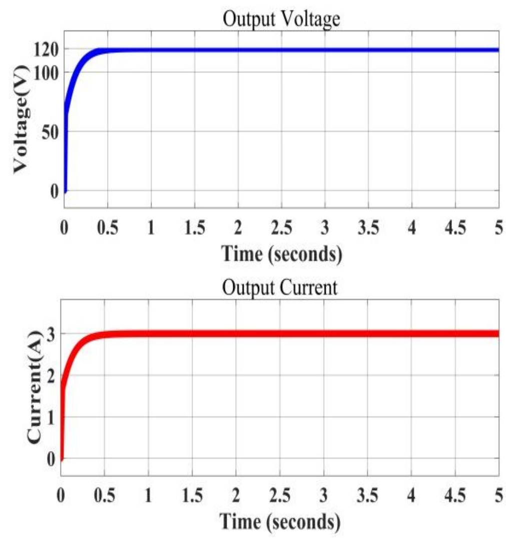

(a)

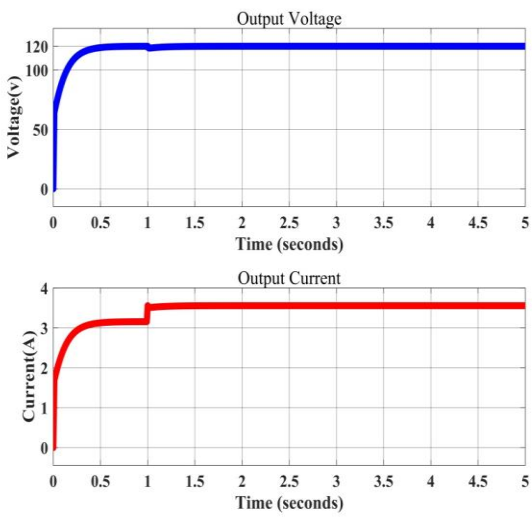

(b)

Fig. 8. Output voltage and output current a) Under a constant load. b) Under step load change.

In mode 3, during high sunshine days the battery will be moved towards non operating mode and solar PV entirely supplies power to the vehicle which energies the inductor L_1.

The charging voltage and current are depicted in Fig 7e, output voltage and current are shown in Fig 7f. The simulation results confirm that the converter operation matches the requirements from the dual source to load.

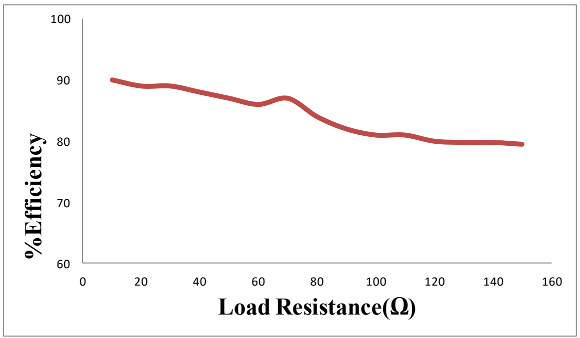

Fig. 9. Efficiency Vs Output Resistance.

The relevant waveform for dynamic mode of operation of DINISC is shown in Fig.8b A step load change at time t=1s is shown and a voltage of 120volts is been regulated for this dynamic condition. The waveform from Fig 8 shows that the DINISC offers a greater voltage gain.

In mode 4 the charged energy in L_1 is transferred to load through the freewheeling diode. From the Fig.7b, it is clearly observed that output voltage is 120V and the output current is around 3A.

Table 3. Comparison of Different Dual Input converter Topologies.

Description	Proposed	Sivaprasad Athikkal et.al., (2017)	Binxin Zhu et.al., (2019)	Venkata et al., (2016)
No. of inputs	2	2	2	2
No. of switches	3	4	2	2
Diodes	3	1	2	2
Inductor	2	1	2	2
Capacitor	2	1	2	5
Number of possible modes of operation	4	6	1	1
Simultaneous power supply from both the sources	Yes	Yes	No	No
Output	Non inverted	Inverted	Non inverted	Non inverted

Finally, the value of efficiency for different load conditions is depicted in Fig 9, from the figure it can be concluded that proposed DINISC have better efficiency

Performance analysis of DINISC, The voltage gain of the converter is about 1.7 to 2.5 with a better efficiency throughout all modes of operations under dynamic load conditions. The performance comparison of DINISC has been carried out with other Multi input converters. From Table 3, a comparison is made based on number of components, simultaneous operation, type of output and modes of operation, it is clearly observed that the proposed converter is comparatively good when compared with other converters reported in the literature. Furthermore, the added advantage towards the selection of proposed converter will produce a non inverted output to the EV motor drive.

The converter can be implemented in real time with minimal reduction in efficiency owing to parasitic effects, switching losses, and thermal effects. The thermal effect can be controlled by proper heat sink arrangement and other abnormalities can be overcomed, through proper optimized design.

7. CONCLUSION

A dual input charging can be provided to the EV motor with simultaneously charging and supports a pollution free atmosphere. The need for an extra inverse amplifier circuit when compared to buck-boost type converter can be eliminated in the DINISC which makes the system cost-effective and efficient. This is a significant advantage in terms of design complexity and overall system cost. The Eigen-values of the system matrix obtained using state space averaging show that the system is stable. Since the main essence of the work is on theoretical models and simulation. The effectiveness of simulation is verified using MATLAB/SIMULINK environment under constant and dynamic load conditions whose dual input of 24V &48V to produce an output of 120V.The efficiency analysis of the converter validates that it has better performance and also the voltage gain of the proposed converter is high. In the future, the proposed methodology will be implemented in a real-time hardware setup. The simulated converter can be utilised to any three or four wheeler application in which the proposed converter can actively adapt to fuel cell with solar PV combination or solar PV with wireless inductive charging to provide continuous power to the load.

REFERENCES

Alexis Kwasinski., (2009). Identification of Feasible Topologies for Multiple-Input DC–DC Converters. *IEEE Transactions on Power Electronics,* 24(3), 856-861.

Ankit Kumar Singh, Anjanee Kumar Mishra, Krishna Kumar Gupta, Pallavee Bhatanagar, Taehyung Kim.,(2020). An Integrated Converter with Reduced Components for Electric Vehicles Utilizing Solar and Grid Power Sources. *IEEE Transactions on Transportation Electrification*, 6(2), 439-452.

Ankul Gupta, Rajapandian Ayyanar, Sombuddha Chakraborty.,(2021). Novel Electric Vehicle Traction Architecture with 48 V Battery and Multi-Input, High Conversion Ratio Converter for High and Variable DC-Link Voltage. *IEEE Open Journal of Vehicular Technology,* 2(1), 448-470.

Arun S, Imthias Ahamed T.P., Z.V. Lakaparampil., (2023). A SEPIC-based three-port converter system using a mode-specific power flow management control for solar energy harvesting. *Renewable Energy Focus*, 44(1), 56–74.

Binxin Zhu, Qingdian Zeng, Don Mahinda Vilathgamuwa, Yang Li, Xiaoli She.,(2019). Non-isolated high-voltage gain Dual -input DC/DC converter with a ZVT auxiliary circuit. *IET Power Electronics,* 12(4), 627-965.

Gangavarapu Guru Kumar, Kumaravel Sundaramoorthy , Sivaprasad Athikkal , Venkitusamy Karthikeyan.,(2019). Dual input super boost DC–DC converter for solar powered electric vehicle. *IET Power Electronics*, 12(9), 2276-2284.

Gangavarapu Guru Kumar, Kumaravel Sundaramoorthy, Sivaprasad Athikkal.,(2022).Dual-Input Non isolated DC–DC Converter With Vehicle-to-Grid Feature. *IEEE Journal of Emerging and Selected Topics in Power Electronics,*10 (3), 3324-3336.

Kuditi Kamalapathi, Panugothu Srinivasa Rao Nayak, Vipul Kumar Tyagi., (2021). Design and implementation of dual-source (WPT + PV) charger for EV battery charging. *International Transactions on Electrical Energy Systems,* 12(9), 2276-2284.

Lalit Kumar, Shailendra Jain.,(2013). Multiple-input DC/DC converter topology for hybrid energy system, *IET Power Electronics*,6(8), 1483–1501.

Luis M. Fernandez, Pablo Garcia, Carlos Andrés Garcia, Francisco Jurado.,(2011). Hybrid electric system based on fuel cell and battery and integrating a single dc/dc converter for a tramway. *Energy Conversion and Management,* 52(5), 2183- 2192.

M.A. Hannan, F.A. Azidin, A. Mohamed., (2021).Hybrid electric vehicles and their challenges: A review. *Renewable and Sustainable Energy Reviews*, 29(1), 135-150.

Maheswari Ellappan, Kavitha Anbukumar., (2020). Comparative Analysis of ACM and GPWM Controllers in Continuous Input and Output Power Boost PFC Converter. *Journal of Control Engineering and Applied Informatics,* 22(4), 61-70.

Michelangelo Grosso, Davide Lena , Alberto Bocca , Alberto Macii , Salvatore Rinaudo.,(2016). Energy-efficient battery charging in electric vehicles with solar panels. *IEEE 2nd International Forum on Research and Technologies for Society and Industry Leveraging*.

Moumita Pramanik , Hiranmay Samanta , Sudipta Basu Pal , Konika Das Bhattacharya , Chandan Kumar Chanda, Hiranmay Saha .,(2023).Onboard Rooftop Solar Charging for Green Transportation in tourism sector. *2023 IEEE IAS Global Conference on Renewable Energy and Hydrogen Technologies (GlobConHT) Male, Maldives*, 1-6.

Muhammad Hosnee Mobarak , Rafael N. Kleiman , and Jennifer Bauman.,(2020).Solar-Charged Electric Vehicles: A Comprehensive Analysis of Grid, Driver, and Environmental Benefits. *IEEE Transactions on Transportation Electrification*, 7(2), 579-603.

Paul Arévalo, Antonio Cano, Javier Benavides, Francisco Jurado.,(2021). Feasibility study of a renewable system (PV/HKT/GB) for hybrid tramway based on fuel cell and super capacitor. *IET Renewable Power Generation,* 15,491-503.

Robert W. Erickson and Dragan Maksimovic, (2004). *Fundamentals of Power Electronic.*213-247, Springer US.

Saikumar Bairabathina, Balamurugan Subraman.,(2023). Design, prototype validation, and reliability analysis of a multi-input DC/DC converter for grid-independent hybrid electric vehicles. *International journal of circuit theory and applications,* 51(5), 2375-2405.

Sanjida Moury, John Lam,(2021). A Soft-Switched, Multiport Photovoltaic Power Optimizer with Integrated Storage Interface and Output Voltage Regulation. *IEEE Transactions on Industrial Electronics* 68(5), 3917-3927.

Sivaprasad Athikkal, Gangavarapu Guru Kumar,, Kumaravel Sundaramoorthy, Ashok Sankar.,(2017). Performance Analysis of Novel Bridge Type Dual Input DC-DC Converters. *IEEE Access*, 5 , 15340-15353.

Venkata Anand Kishore Prabhala, Poria Fajri, Venkat Sai Prasad Gouribhatla, Bhanu Prashant Baddipadiga, and Mehdi Ferdowsi.,(2016). A DC–DC Converter with High Voltage Gain and Two Input Boost Stages. *IEEE Transactions on Power Electronics*, 31(6), 4206-4215.

Yan Li, Xinbo Ruan, Dongsheng Yang, Fuxin Liu and Chi K. Tse.,(2010).Synthesis of Multiple-Input DC/DC Converters. *IEEE Transactions on Power Electronics,* 25(9), 2372-2385.